

Contents lists available at ScienceDirect

# Journal of Membrane Science

journal homepage: http://www.elsevier.com/locate/memsci





# Enhancing air-dehumidification performance of polyimide membranes by generating hydrophilic Poly(amic acid) domains using partial hydrolysis

Sunghwan Park a, Hae-Kwon Jeong a,b,\*

- a Artie McFerrin Department of Chemical Engineering and, Texas A&M University, 3122 TAMU, College Station, TX, 77843-3122, United States
- b Department of Materials Science and Engineering, Texas A&M University, 3122 TAMU, College Station, TX, 77843-3122, United States

#### ARTICLE INFO

Keywords:
Polyimide
Poly(amic acid)
Hydrolysis
Air-dehumidification membrane

#### ABSTRACT

Membrane-based air-dehumidification has been considered as one of the most promising technologies for the next-generation heating, ventilation, and air-conditioning (HVAC) systems. Though attractive, polymeric membranes suffer from limitation between their  $H_2O/N_2$  separation performance (i.e.,  $H_2O/N_2$  separation factor and  $H_2O$  permeability) and their mechanical stability. Herein, we propose a facile and effective strategy, controlled partial hydrolysis, to improve the  $H_2O/N_2$  separation performance of polyimide (PI) membranes while maintaining their mechanical stability. Controlled hydrolysis turned the PI membranes partially into poly (amic acid) (PAA)/PI membranes, exhibiting an asymmetric configuration with the inner layers more hydrolyzed. Interestingly, the hydrolysis in a highly concentrated NaOH solution led to formation of localized domains that were hydrolyzed (i.e., PAA domains). The localized hydrolysis of mechanically stable PI membranes led to formation of hydrophilic PAA channels embedded in the PI, thereby enhancing  $H_2O/N_2$  separation performance (i.e.,  $H_2O$  permeability from  $\sim 6400$  Barrer to  $\sim 11,000$  Barrer and  $H_2O/N_2$  separation factor from  $\sim 190$  to  $\sim 320$ ) while preserving the mechanical strength of the membranes.

# 1. Introduction

Heating, ventilation, and air-conditioning (HVAC) systems are essential in our daily life. Tremendous energy is, however, consumed and the demand for HVAC increases continuously all over the world [1]. Residential and commercial buildings in U.S. consumed more than 76% of total electricity and  $\sim\!35\%$  of total energy (i.e., 13.45 quadrillion Btu) for HVAC [2]. In addition, the current air cooling and dehumidification of more than 90% relies on vapor compression system using synthetic refrigerants, hydrofluorocarbons (HFCs), which are most potent greenhouse gases [3]. The high energy consumption of the current HVAC systems combined with its adverse impacts on environment requires urgent needs for a next-generation HVAC technology.

There have been several potential technologies for the future HVAC system such as thermoelastic [4,5], membrane [6,7], desiccant [8,9], and etc. Among them, membrane-based air dehumidification technology has been considered as one of the most promising next-generation HVAC technologies by U.S. Department of Energy (U.S. DOE) [10]. Membrane-based air dehumidification does not require an additional heat source, regeneration, and emission of greenhouse gases. Air-dehumidification by membranes can be carried out at a constant

temperature by a chemical potential gradient of water vapor between two sides of a membrane generated by a vacuum pump [11]. The efficiency of isothermal membrane-based air-dehumidification (IMAD) has been demonstrated by incorporating membranes in hybrid HVAC systems. The combination of a membrane with a desiccant-based system increased the efficiency by 30% owing to reduced cooling load variation (i.e., extent of difference between minimum and maximum cooling loads) [12]. Also, comparing with conventional stand-alone vapor compression systems, membrane/evaporative hybrid cooling systems showed up to 86.2% greater efficiency with respect to energy saving [13]

Since the efficiency of the IMAD depends on separation performances of membranes, it is highly desirable to develop membranes with enhanced  $\rm H_2O$  permeability and  $\rm H_2O/air$  ( $\rm H_2O/N_2$ ) selectivity [14]. Liu et al. [11] evaluated that the  $\rm H_2O/N_2$  separation factor of 200 is minimally required to satisfy the coefficient of performance (COP) 50% greater than the vapor compression system as proposed by U.S. DOE. Several different types of membranes have been reported to achieve high  $\rm H_2O/N_2$  separation performance including polymer [15], zeolite [11], polymer/inorganic hybrid [16,17], and hygroscopic liquids [18, 19]. Especially, polymeric membranes have been widely used and

<sup>\*</sup> Corresponding author. Department of Chemical Engineering and, Texas A&M University, 3122 TAMU, College Station, TX, 77843-3122, United States. E-mail address: hjeong7@tamu.edu (H.-K. Jeong).

extensively studied for practical applications due to their relatively low cost and ease processability [6].

The hydrophilicity of polymeric materials plays a critical role in increasing both H<sub>2</sub>O permeability and H<sub>2</sub>O/N<sub>2</sub> selectivity simultaneously by enhancing their affinity with water vapor. In many cases of air-dehumidification membranes, however, excessive hydrophilicity can lead to low mechanical property, thereby resulting in poor stability. Hence, the majority of the polymers for air-dehumidification were optimized for maximum enhancement in their hydrophilicity and minimum loss in their mechanical stability. Poly (ethylene oxide) poly (butylene terephthalate) (PEO-PBT) copolymer showed both stability and high H<sub>2</sub>O/N<sub>2</sub> separation performance (i.e., H<sub>2</sub>O permeability of 8.5  $\times 10^4$  Barrer and  $H_2O/N_2$  selectivity of  $4 \times 10^4$ ) [15]. The high and stable separation performance of the membranes was achieved by the hydrophilicity of permeable hydrophilic PEO blocks (56%) and the mechanical stability of impermeable hydrophobic PET blocks (44%) [15]. Similarly, Pebax®MV1074 made of 45% of rigid hydrophobic nylon 12 (PA12) blocks and 55% of soft hydrophilic PEO blocks exhibited relatively high H<sub>2</sub>O permeability of 1.6 x 10<sup>5</sup> Barrer and H<sub>2</sub>O/N<sub>2</sub> selectivity of 2 x 10<sup>5</sup> [20]. Sulfonated poly (ether ketone) (SPEEK) with an optimal sulfonation degree of 60% showed high H<sub>2</sub>O permeability of 6 x 10<sup>4</sup> Barrer and exceptional  $H_2O/N_2$  selectivity of 1 x  $10^7$  [20,21].

4,4'-(Hexafluoroisopropylidene)diphthalic anhydride (6FDA)-based polyimide (PI) polymers have been extensively studied for gas separation due to their high free volume stemming from their bulky trifluoromethyl (-CF<sub>3</sub>) pendent groups, thereby showing high gas permeabilities [22]. In particular, 2,4,6-trimethyl-1,3-diaminobenzene (DAM) or 2,3,5,6-tetramethyl-1,4-phenylenediamine (durene) moieties in 6FDA-PIs provides exceptionally high gas permeabilities due to enlarged excess free volume [23,24]. Furthermore, the imide and aromatic rings provide outstanding thermal and mechanical stabilities [25, 26]. Despite the extensive studies for gas separation membranes, 6FDA-PI has yet to be investigated for IMAD applications due to their relative hydrophobic property. Hydrophobic PI, nonetheless, can be transformed to hydrophilic poly (amic acid) (PAA) through a simple hydrolysis reaction [27], potentially leading to formation of hydrophilic/hydrophobic PAA/PI membranes for stable air-dehumidification.

In this work, we investigated controlled transformation of 6FDA-based PI membranes into PAA/PI membranes by partial hydrolysis for IMAD applications. The partial transformation of the hydrophobic imide rings of the PI membranes to the hydrophilic amide groups and carboxylic salt groups improved their  $\rm H_2O/N_2$  separation performance while maintaining their mechanical robustness. The partial hydrolysis of PI membranes to PAA/PI membranes was controlled by changing the reaction conditions such as solution concentrations, reaction times, and reaction rates. The physical/chemical properties of the resulting membranes were characterized and their  $\rm H_2O/N_2$  separation performances were measured.

### 2. Experimental

### 2.1. Materials

6FDA-DAM (4,4-(Hexafluoroisopropylidene) diphthalic anhydride 2,4,6-trimethyl-1,3-phenylenediamine, Mw: 148k, PDI: 2.14) was purchased from Akron Polymer Systems Inc. N,N-dimethylformamide (DMF) ( $C_3H_7NO>99.8\%$ , Alfa Aesar) was used as a solvent to dissolve the polymer. For hydrolysis, sodium hydroxide (NaOH > 97.0%, VWR Chemicals BDH®) and sodium formate (HCOONa  $\geq 99\%$ , Sigma Aldrich) were used. Copper (II) nitrate trihydrate (Cu (NO<sub>3</sub>)<sub>2</sub>·3H<sub>2</sub>O,  $\geq$  99%, Sigma Aldrich) and lithium nitrate (LiNO<sub>3</sub>  $\geq$  99%, Acros Organics) were used for ion exchange.

# 2.2. Preparation of $\alpha$ -alumina supports

 $\alpha$ -alumina disks were as supports and prepared by following a recipe

previously published [28]. In short,  $\alpha$ -alumina powder (CR6, Baikowski) was mixed with a polyvinyl alcohol (PVA) binder solution. The binder solution was prepared by mixing 3 g of PVA500 (Mw: 22k, Duksan) and 5 ml of 1 M HNO<sub>3</sub> in 95 ml of D.I. water. A proper amount of the powder was put into a mold and pressed uniaxially with 200 bar, forming an  $\alpha$ -alumina disk. The  $\alpha$ -alumina disk was sintered at 1100 °C for 2 h at the ramp rate of 5 °C min<sup>-1</sup>. After that, the disk was polished by a sandpaper (grid #1200) to smoothen its surface. The dimensions of the prepared  $\alpha$ -alumina disk were 2.2 cm in diameter, 2 mm in thickness, and 46% in porosity with an average pore diameter of ~200 nm.

# 2.3. Fabrication of polymer films

0.25 g of 6FDA-DAM was dissolved in 12.25 g of DMF to prepare a 2 wt% polymer dope solution. 2.0 ml of the polymer dope solution was dropped on the polished side of an  $\alpha\text{-alumina}$  disk using a micropipette, fully covering the support surface. Immediately, the sample was transferred into a vacuum oven pre-heated at  $150~^\circ\text{C}$  and soaked at the same temperature for 24~h under vacuum. Afterward, the sample was cooled down to room temperature. The resulting alumina-supported PI film showed the uniform film thickness of  $6.3\pm1.7~\mu\text{m}$ .

# 2.4. Hydrolysis of PI films

Two different hydrolysis reactions were carried out. For NaOH-induced hydrolysis, a PI film was hydrolyzed by immersing in a NaOH aqueous solution at various NaOH concentrations (i.e., 1, 2, 3, and 4 M) at room temperature for 1 min. Immediately after, the sample was washed with D.I. water overnight and then dried at 60 °C for a day. For NaCOOH-induced hydrolysis, a PI film was hydrolyzed in a NaCOOH solution (100 mmol of NaCOOH in 30 ml of D.I. water) at 120 °C for various reaction times (i.e., 6, 9, and 12 h). The sample was vertically loaded on a custom-made Teflon holder and placed in a Teflon-lined autoclave containing the NaCOOH solution. After cooling down to room temperature, the hydrolyzed polymer film was washed with D.I. water overnight. The sample was then dried at 60 °C for a day.

# 2.5. Plasma etching

Oxygen plasma etching of films was performed by a plasma cleaner (PDC-32G, Harrick Plasma) under vacuum. The air flow rate was adjusted to obtain the maximum intensity of plasma.

# 2.6. Ion exchange

A hydrolyzed membrane was immersed for 3 h into 1 M Cu $^{2+}$  (or Li $^{+}$ ) aqueous solution prepared by dissolving 24.16 g of Cu(NO<sub>3</sub>) $_2\cdot 3H_2O$  for Cu $^{2+}$  exchange (or 6.90 g of LiNO<sub>3</sub> for Li $^{+}$  exchange) in 100 ml of D.I. water. The sample was washed twice in D.I. water overnight. The washed sample was then dried at 60 °C.

# 2.7. Characterizations

Scanning electron microscope (SEM) images were taken using a JEOL JSM-7500F at working distance of 15 mm and acceleration voltage of 5 keV. Samples for SEM were prepared by freeze fracturing in liquid nitrogen. Composition analysis was performed an energy-dispersive X-ray spectrometry (EDS) (Oxford EDS system) operating at working distance of 8 mm and acceleration voltage of 20 keV with secondary electron image (SEI) detector. Attenuated total reflectance Fourier transform infrared (ATR-FTIR) spectra were taken by a Nicolet iS5 spectrophotometer equipped with iD7 ATR (Thermo Scientific) in the range of 4000–400 cm<sup>-1</sup> at a resolution of 2 cm<sup>-1</sup> with 16 scans. Contact angle measurements were carried out using a microscope camera (Motic Moticam 1000) and were analyzed using ImageJ software. Optical micrographs were taken using a microscope (Axio Imager A1m, Carl Zeiss).

#### 2.8. Permeation measurement

H<sub>2</sub>O/N<sub>2</sub> separation performance of membrane was measured by the custom-made permeation measurement system presented in Fig. S1. The humidified feed flow was prepared by mixing a proper ratio of dry N2 and water-saturated N2. The feed flow rates were controlled by needle valves with the total flow rate of 200 cm<sup>3</sup> min<sup>-1</sup> and were monitored by mass flow controllers (MFC, DFC, AALBORG). The feed pressure was maintained at 1.5 bar using a back-pressure regulator equipped on the retentate side. The relative humidity and temperature of the feed flow were kept at > 95% and 35 °C, respectively, and were monitored by dew point meters (HMP7, Vaisala). The permeate side was preserved under vacuum condition (i.e., ~0.03 bar) using a diaphragm pump (N 820.3 FTP, KNF). Not to underestimate the performances by water vapor adsorbed onto the downstream membrane/support surfaces, the argon sweep gas was provided to the permeate side of the membrane cell with a flow rate of 50 cm<sup>3</sup> min<sup>-1</sup>. The composition of the permeated flow was determined using a gas analyzer (QGA, Hiden Analytical) and the permeated flow rate was measured by a bubble flow meter. The permeability of component  $i(P_i)$  was calculated using the following

$$P_{i} = \frac{\dot{n}_{p} \times x_{p,i} \times l}{A(p_{f} \times x_{f,i} - p_{p} \times x_{p,i})}$$

where,  $\dot{n}$  is the total flow rates,  $x_i$  is the mole fractions of component i, l is the membrane thickness, A is the area of the membrane, p is the pressure, and the subscripts p and f represents the permeate side and feed side, respectively. The separation factor  $(a_{ij})$  was obtained using the equation below:

$$\alpha_{ij} = \frac{x_{p,i}/x_{p,j}}{x_{f,i}/x_{f,j}}$$

### 3. Results and discussion

# 3.1. Hydrolysis of 6FDA-DAM polyimide membranes

A 6FDA-DAM polyimide (PI) film was prepared by drop-casting on a porous  $\alpha$ -alumina substrate with thickness of 6.3  $\pm$  1.7  $\mu$ m. The PI film was partially hydrolyzed in a NaOH aqueous solution, turning a part of the film into 6FDA-DAM poly (amic acid) (PAA). As shown in Fig. 1, the hydrolysis reaction involves nucleophilic hydroxides attacking the

**Fig. 1.** Hydrolysis of 6FDA-DAM PI to 6FDA-DAM PAA in a NaOH aqueous solution.

carbonyl carbons of the imide rings, thereby breaking the imide rings [29], forming hydrophilic amide groups and carboxylic salt groups coordinated with sodium ions (Fig. 1). There are various variables affecting the hydrolysis reaction including pH, time, temperature, and concentration [29].

The hydrolysis was performed by immersing the PI film facing up in 1 M NaOH aqueous solution. The degree of hydrolysis (i.e., degree of deimidization) was investigated as a function of the film depth by carefully etching the polymer layer using oxygen plasma. As shown in Fig. 2, the intensities of the peaks at 1723 cm $^{-1}$  and 1356 cm $^{-1}$  corresponding to C $\stackrel{}{-}$ O and C $^{-}$ N of the imide ring, respectively, decreased as compared to that of C $^{-}$ C of the benzene ring at 1485 cm $^{-1}$  as the film thickness reduced by the etching [30]. The degree of deimidization (DD) was determined as follows [30,31].

$$\label{eq:DD} \text{Degree of deimidization } (\text{DD})(\%) = \left[1 - \frac{(I_{1356}/I_{1485})_{\textit{specimen}}}{(I_{1356}/I_{1485})_{\textit{standard}}}\right] \times 100$$

Where, *I* is the FT-IR peak intensity and subscripts 1356 and 1485 are the wavenumbers of the peaks of C–N of the imide ring and C–C of the benzene ring, respectively. As the polymer layer was etched from the top surface, the DD linearly increased, indicating the gradual hydrolysis (Fig. S2), suggesting more hydrolysis in the bottom layer than in the top layer (hereafter denoted as asymmetric hydrolysis). This was unexpected given that the top layer was in direct contact with the base solution while the bottom layer was in contact with the alumina support. It is noteworthy here that the oxygen plasma did not affect the DD (see Fig. S3).

A couple of hypotheses can be made to explain the asymmetric hydrolysis (i.e., more hydrolysis in the bottom side than in the top side) as illustrated in Fig. 3. One is that the hydroxide solution absorbed in the porous support was not fully removed from the pores of the support even after the washing step immediately followed by the hydrolysis (Fig. 3a), thereby leading to further hydrolysis of the bottom layer [29,32,33]. The other hypothesis is that the PI film was saturated with the hydroxide solution and then the washing step generated the concentration gradient of the hydroxide since the top layer was in direct contact with the washing solution (Fig. 3b). The hydroxide concentration gradient may cause the asymmetric hydrolysis [29,33]. To check the first hypothesis, hydrolysis was carried out under the same condition for a PI film coated on a non-porous glass substrate with the similar film thickness. Interestingly, the bottom layer was found more hydrolyzed than the top layer as in the case of the film coated on a porous support. The DD values of the top and bottom layers of the hydrolyzed film coated on a non-porous substrate were 14  $\pm$  3% and 23  $\pm$  5%, respectively (Fig. S4), suggesting the second hypothesis is more likely. To further verify the second hypothesis, it was assumed that when the hydrolysis reaction rate is low, the reaction rate would be relatively uniform in the polymer at a fixed reaction time. In this regard, the PI films were hydrolyzed in a weakly basic NaCOOH aqueous solution (3.3 M) at 120 °C for 6 h. The films were found more uniformly hydrolyzed (DDs of the top and bottom layers  $\sim$  19% and  $\sim$ 13%, respectively, see Fig. S5) as compared to those hydrolyzed in an NaOH solution (hereafter denoted as symmetric hydrolysis). Based on these observations, the second hypothesis was confirmed more plausible for the asymmetric hydrolysis. Hereafter, samples hydrolyzed asymmetrically and symmetrically were denoted as A-PAA-nM (n molarity of NaOH solution) and S-PAA-mH (m hours of hydrolysis in NaCOOH solution), respectively.

# 3.2. Effect of different hydrolysis conditions

To achieve more hydrophilic membranes while preserving both structures (asymmetric or symmetric) and sample integrity, the concentration of the NaOH solution was increased to 1, 2, 3, and 4 M for a fixed reaction time (1 min) for asymmetric hydrolysis while the hydrolysis reaction time was prolonged to 6, 9, and 12 h in the 3.3 M

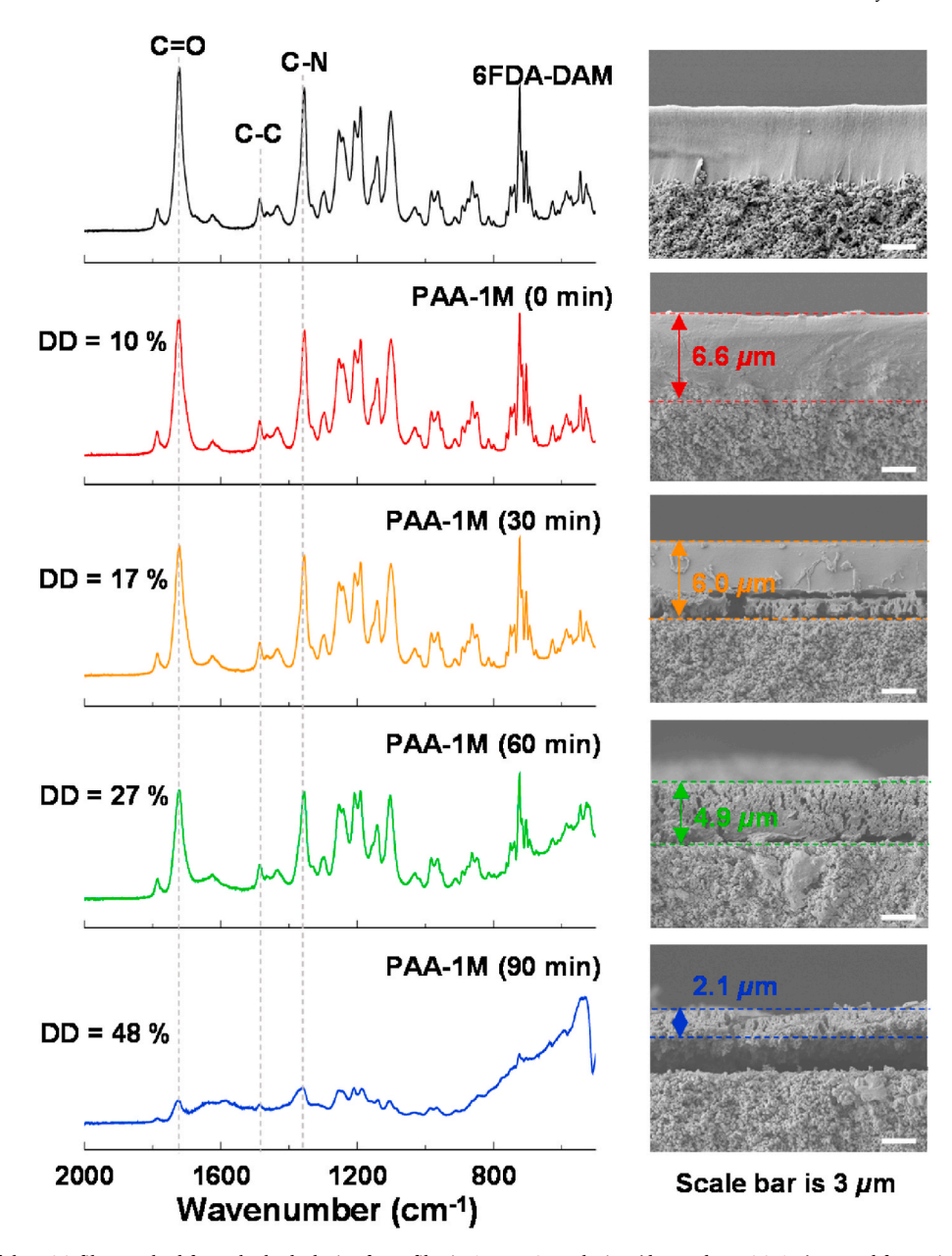


**Fig. 2.** FT-IR spectra of the PAA film resulted from the hydrolysis of a PI film in 1 M NaOH solution (denoted as PAA-1M) treated for various oxygen plasma etching times (n min, n = 0, 30, 60, and 90) and the corresponding SEM images in comparison with those of the PI film.

NaCOOH solution for symmetric hydrolysis. It is noted that too aggressive hydrolysis led to degradation of the polymer, significantly decreasing its mechanical stability [33,34]. The polymer films were found disintegrated when the concentration of the NaOH aqueous solution exceeded 5 M or the hydrolysis time in the NaCOOH solution was longer than 15 h. As the reaction time of the symmetric hydrolysis increased, the surface DD increased from 19% to 38%–71% (Fig. S6a). In contrast, there were no significant changes in the DD of the sample surfaces (i.e., 10, 15, 17, and 16%) as the NaOH concentration increased due to the asymmetric hydrolysis (Fig. S6b).

We attempted to determine how the hydrophilicity of the film was affected by deimidization using contact angle measurements. As shown in Fig. 4 and Fig. S7, the contact angle showed a strong negative correlation with the degree of deimidization for the symmetrically hydrolyzed samples. Though the asymmetrically hydrolyzed samples (A-PAA-2M, A-PAA-3M, and A-PAA-4M) showed similar surface DD (15, 17, 16%, respectively), their contact angles were dramatically decreased ( $\sim$ 68.1,  $\sim$ 28.9 and  $\sim$ 13.4°, respectively). In other words, the

asymmetrically hydrolyzed samples (A-PAA-3M and A-PAA-4M) exhibited much more hydrophilic surfaces than the symmetrically hydrolyzed sample (S-PAA-9H) given the similar surface DD (Fig. 4 and Fig. S7). This can be attributed due to the localized intense hydrolysis on the sample surfaces (A-PAA-3M and A-PAA-4M). As shown in Fig. S8, it was found that deimidization was not uniform throughout the sample surface (A-PAA-4M). In other words, there were regions on the surface, exhibiting relatively high DD. One plausible explanation is that when the NaOH concentration was sufficiently high, there might be accelerated hydrolysis on those regions, thereby leading to formation of percolation pathways (Fig. 5). Hence, the regions containing percolation pathways on the surface exhibited relatively high DD, thereby more hydrophilic with lower contact angle.

To confirm the presence of hydrophilic percolation pathways, the asymmetrically hydrolyzed samples were dyed with  $\text{Cu}^{2+}$ , which has a light blue color, via an ion exchange. Due to the higher charge density, they can readily exchange the Na $^+$  ions coordinated to the PAA [35]. Accordingly, it was expected that the regions where percolation

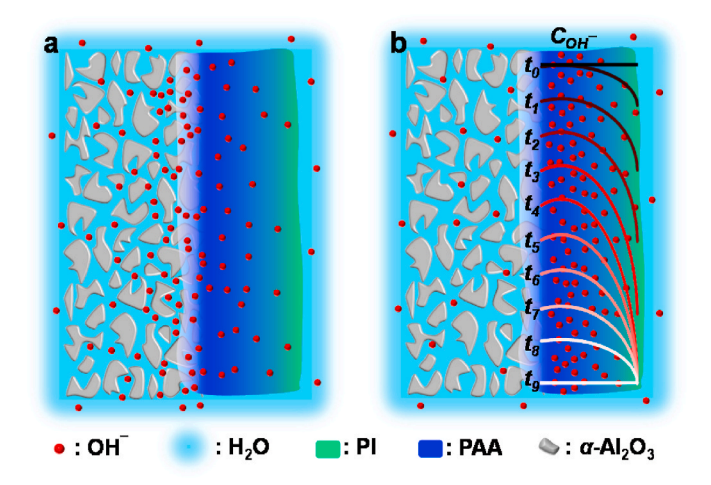


**Fig. 3.** Illustrations of two hypotheses proposed for asymmetric hydrolysis: high NaOH concentration at the bottom due to (a) the excess NaOH in the support pores and (b) the removal of NaOH from the top surface during the washing step.

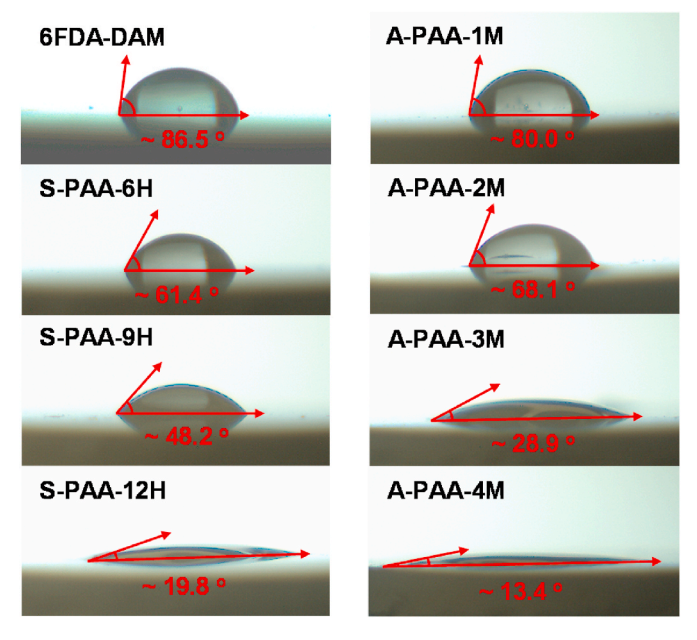


Fig. 4. Contact angle measurements for a water droplet.

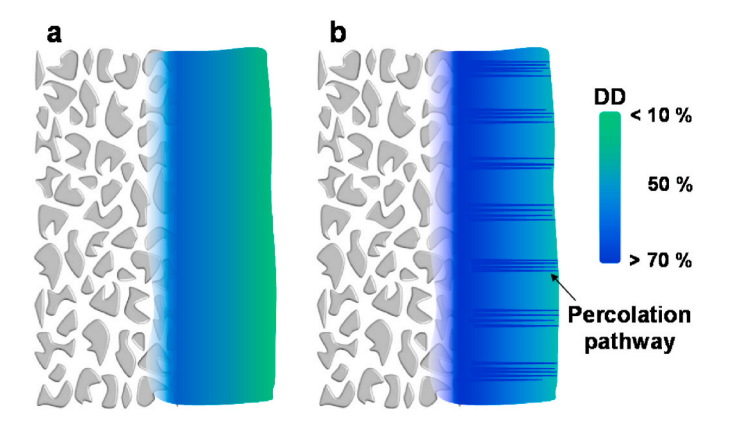


Fig. 5. Illustrations of asymmetrically hydrolyzed PAA samples at a low NaOH concentration (a) and a high NaOH concentration (b).

pathways were present would exhibit more intense blue color due to the higher concentrations of Cu<sup>2+</sup> ions present than the other regions. Indeed, upon Cu<sup>2+</sup> exchange, the PAA samples showed color change (Fig. S9). Fig. 6 presents the optical micrographs of the samples hydrolyzed under different conditions. The symmetrically hydrolyzed S-PAA-12H was uniformly blue throughout its surface (Fig. 6a), indicating rather uniform hydrolysis. In a stark contrast, the samples hydrolyzed asymmetrically (Fig. 6b-f) exhibited dispersed spots in more intense blue color, suggesting nonuniform hydrolysis. The higher the NaOH concentration the more intense the color of the dispersed blue spots (Fig. 6b-f). Interestingly, there were parts of the surface of the A-PAA-4M sample that displayed more drastic contrast (see Fig. 6f), clearly showing the presence of percolation pathways. In other words, the more clear and intense color of the dispersed spots from some parts of the sample (Fig. 6f) comparing with the other parts of the sample (Fig. 6e) strongly suggested presence of the more hydrolyzed regions on the surface. In addition, the EDS mapping of A-PAA-4M showed Cu<sup>2+</sup> doped channels through the membrane (Fig. \$10), indicating the pathways extended to the sample bottom.

# 3.3. Air-dehumidification performance

Fig. 7 shows the H<sub>2</sub>O/N<sub>2</sub> separation performance of the PAA membranes asymmetrically hydrolyzed under different NaOH concentrations (see Table S1 for numerical values). As the NaOH concentration increased, the H<sub>2</sub>O permeability and the H<sub>2</sub>O/N<sub>2</sub> separation factor of the membranes were improved simultaneously. This indicated that the increase in hydrophilicity resulting from the increase in the PAA fractions enabled the faster H<sub>2</sub>O permeation possibly due to the enhanced H<sub>2</sub>O solubility of the PAA samples. On the other hand, the N<sub>2</sub> permeability remained relatively unchanged although reduced free volume by partial hydrolysis might decrease diffusion of both N2 and H2O [36]. This was likely due to the enhanced chain flexibility and the swelling by H2O molecules saturated in the PAA domains. Particularly, the samples hydrolyzed with the higher NaOH concentrations (i.e., A-PAA-3M and A-PAA-4M) displayed more dramatic enhancement in their H<sub>2</sub>O/N<sub>2</sub> separation performance. This was likely due to the enhanced chain flexibility and the swelling by H2O molecules saturated in the PAA domains [37]. The A-PAA-4M showed  $\sim 70\%$  enhancement in  $H_2O$ permeability upon the partial hydrolysis, which was comparable or superior to those of the composite membranes reported [38,39]. It was surmised that the percolation pathways provided low H<sub>2</sub>O transport resistance, thereby enabling facile H<sub>2</sub>O transport across the membranes. Furthermore, the improved air-dehumidification performance was relatively well preserved for two weeks despite a slight decrease in the H<sub>2</sub>O permeability possibly due to the aging effect (Fig. S11) [40].

Comparing with asymmetrically hydrolyzed PAA films (A-PAA), the symmetrically hydrolyzed samples (S-PAA) showed moderate and more gradual separation performance enhancements as the degree of hydrolysis increased (Table S1 and Fig. S12). The A-PAA samples hydrolyzed under relatively mild hydrolysis conditions showed the similar contact angle as the S-PAA samples and exhibited H2O/N2 separation performance comparable with S-PAA. When hydrolyzed under relatively severe conditions, despite their similar contact angles as S-PAA, the A-PAA samples (i.e., A-PAA-3M and A-PAA-4M) displayed H<sub>2</sub>O/N<sub>2</sub> separation performance largely deviating from the S-PAA samples likely due to the formation of percolation pathways. The percolation pathways present in the A-PAA samples provided the lower resistance to H<sub>2</sub>O transport, allowing more selective and facile H2O permeation than the more uniformly hydrolyzed S-PAA. Furthermore, symmetrical hydrolysis (S-PAA) led to the formation of defects when the DD exceeded  ${\sim}70\%$  (i.e., hydrolysis time longer than  $\sim 15$  h). In other words, the symmetrically hydrolyzed samples consisting of uniformly mixed PAA and PI phases became mechanical unstable at higher PAA fractions. However, the asymmetrically hydrolyzed samples led to formation of the PAA-rich domains (i.e., percolation pathways) randomly dispersed in the PI-rich

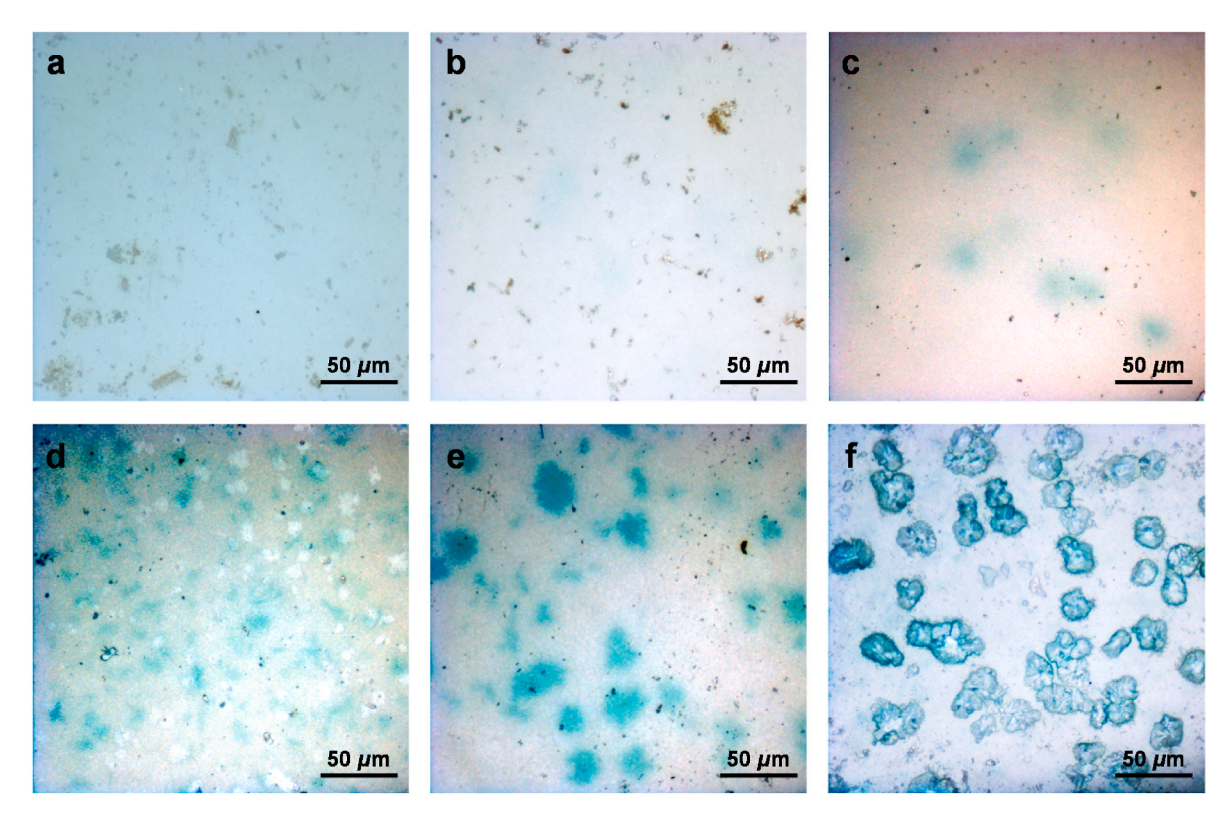


Fig. 6. Optical micrographs of (a) S-PAA-12H, (b) A-PAA-1M, (c) A-PAA-2M, (d) A-PAA-3M, (e) A-PAA-4M with less hydrolyzed region, and (f) A-PAA-4M with more hydrolyzed region.

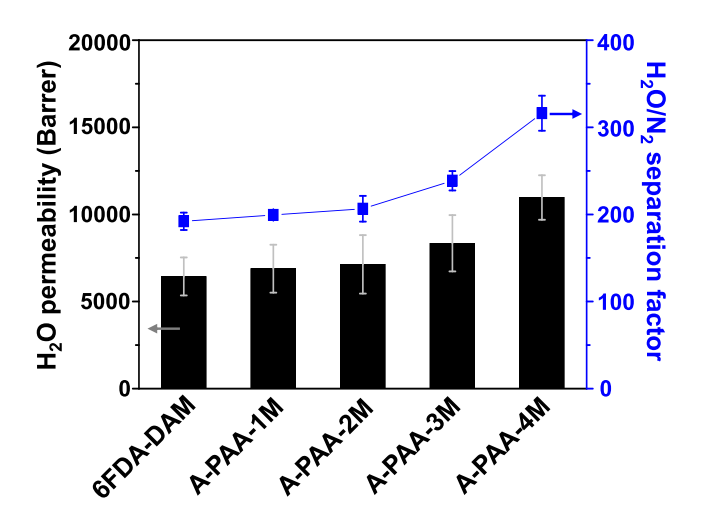


Fig. 7.  $\rm H_2O/N_2$  separation performance of 6FDA-DAM and asymmetrically hydrolyzed A-PAA samples.

domains, thereby ensuring the integrity of the films. The A-PAA samples with highly hydrophilic channels dispersed in the robust PI-rich domains were found to exhibit better microstructures to achieve more improved air-dehumidification performance compared to the S-PAA.

To investigate the effect of charge-balancing cations in PAA on the membrane performance, two different cations,  ${\rm Li}^+$  and  ${\rm Cu}^{2+}$  ions, were ion-exchanged with Na $^+$  ions in PAA. With Li $^+$  ions, there were no significant changes in the  ${\rm H_2O/N_2}$  separation performance (Fig. 8). With  ${\rm Cu}^{2+}$  ions, however, both  ${\rm H_2O}$  permeability and  ${\rm H_2O/N_2}$  separation factor decreased significantly (Fig. 8). It was found that upon the  ${\rm Cu}^{2+}$  exchange, A-PAA became more hydrophobic as evidenced by the

substantial increase in the contact angles (from  $\sim\!13.4^\circ$  to  $\sim\!67.5^\circ$  for A-PAA-4M and from  $\sim\!19.8^\circ$  to  $\sim\!77.3^\circ$  for S-PAA-12H) (Fig. S13). The decrease in the  $\rm H_2O/N_2$  separation performance of the A-PAA-4M was more predominant than that of the S-PAA-12H (Fig. 8). This might be due to the preferential blocking of the percolation pathways in A-PAA-4M by  $\rm Cu^{2^+}$  ions. Further studies are necessary to elucidate the exact mechanism by which  $\rm Cu^{2^+}$  ions block percolation pathways.

# 4. Conclusion

Here, we showed transformation of 6FDA-based PI membranes into PAA/PI membranes by partial hydrolysis for air-dehumidification under two different hydrolysis conditions, leading to formation of symmetrically (S-PAA) and asymmetrically (A-PAA) hydrolyzed PAA membranes. It was found that asymmetric hydrolysis was enabled by the NaOH concentration gradient along the membrane thickness developed upon washing. Nevertheless, the greater the degree of hydrolysis, the more hydrophilic the membranes, thereby improving their H<sub>2</sub>O/N<sub>2</sub> separation performances. In particular, the A-PAA membranes showed dramatic  $H_2O/N_2$  separation performance enhancement (i.e.,  $\sim 70\%$  increase in  $H_2O$  permeability and ~65% increase in  $H_2O/N_2$  separation factor) due to the presence of exceptionally hydrophilic PAA percolation pathways resulting from localized intense hydrolysis. Comparing with the S-PAA membranes, the presence of percolation pathways in the A-PAA membranes led to 1) further increase in their H2O/N2 separation performances and 2) higher physical stability due to the mechanically-robust PI-rich matrices. Finally, when exchanged with Cu<sup>2+</sup> ions, the A-PAA membranes showed drastically decreased separation performance, likely due to the blockage of the percolation pathways.

### CRediT authorship contribution statement

**Sunghwan Park:** Conceptualization, Experiments, Data Collection/ Analysis, Original draft preparation. **Hae-Kwon Jeong:** 

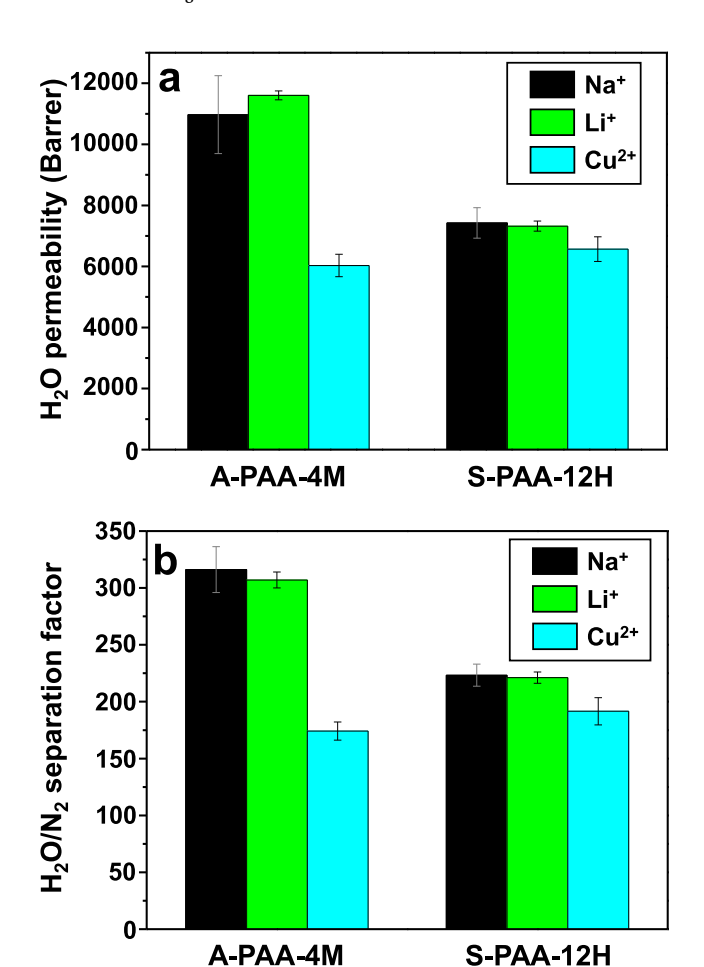


Fig. 8. Comparison of  $\rm H_2O/N_2$  separation performance of PAA with different cations (i.e.,  $\rm Na^+$ ,  $\rm Li^+$ , and  $\rm Cu^{2+}$ ): (a)  $\rm H_2O$  permeability and (b)  $\rm H_2O/N_2$  separation factor.

Conceptualization, Supervision, Writing- Reviewing, and Editing.

#### **Declaration of competing interest**

The authors declare that they have no known competing financial interests or personal relationships that could have appeared to influence the work reported in this paper.

# Acknowledgement

H.-K.J. acknowledges the financial support from the National Science Foundation (CBET-1929596). This publication was made possible in part by NPRP12S-0128-190016 from the Qatar National Research Fund (a member of Qatar Foundation). The findings achieved herein are solely the responsibility of the authors. The National Science Foundation supported the FE-SEM acquisition under Grant DBI-0116835, the VP for Research Office, and the Texas A&M Engineering Experimental Station.

# Appendix A. Supplementary data

Supplementary data related to this article can be found online at  $\frac{\text{https:}}{\text{doi.org}}$  10.1016/j.memsci.2020.119006.

#### References

- [1] L. Wood, Global Heating, Ventilation, and Cooling Markets Report 2019 \$135+ Bn 2014-2018 Analysis & 2019-2024 Forecasts, PRNewswire, Research and Markets, 2019.
- [2] J.J. Conti, P.D. Holtberg, J.R. Diefenderfer, S.A. Napolitano, M. Schaal, J. T. Turnure, L.D. Westfall, U.S. D.O.E, in: Annual Energy Review, 2014. Washington, DC, 2014.
- [3] M.F. Lunt, M. Rigby, A.L. Ganesan, A.J. Manning, R.G. Prinn, S. O'Doherty, J. Muhle, C.M. Harth, P.K. Salameh, T. Arnold, R.F. Weiss, T. Saito, Y. Yokouchi, P. B. Krummel, L.P. Steele, P.J. Fraser, S.L. Li, S. Park, S. Reimann, M.K. Vollmer, C. Lunder, O. Hermansen, N. Schmidbauer, M. Maione, J. Arduini, D. Young, P. G. Simmonds, Reconciling reported and unreported HFC emissions with atmospheric observations, P Natl Acad Sci USA 112 (2015) 5927–5931.
- [4] S.X. Qian, A. Alabdulkarem, J.Z. Ling, J. Muehlbauer, Y.H. Hwang, R. Radermacher, I. Takeuchi, Performance enhancement of a compressive thermoelastic cooling system using multi-objective optimization and novel designs, Int. J. Refrig. 57 (2015) 62–76.
- [5] S.X. Qian, J.Z. Ling, Y.H. Hwang, R. Radermacher, I. Takeuchi, Thermodynamics cycle analysis and numerical modeling of thermoelastic cooling systems, Int. J. Refrig. 56 (2015) 65–80.
- [6] M. Qu, O. Abdelaziz, Z.M. Gao, H.X. Yin, Isothermal membrane-based air dehumidification: a comprehensive review, Renew. Sustain. Energy Rev. 82 (2018) 4060–4069.
- [7] J. Woods, Membrane processes for heating, ventilation, and air conditioning, Renew. Sustain. Energy Rev. 33 (2014) 290–304.
- [8] S. Misha, S. Mat, M.N. Ruslan, K. Sopian, Review of solid/liquid desiccant in the drying applications and its regeneration methods, Renew. Sustain. Energy Rev. 16 (2012) 4686–4707.
- [9] K. Daou, R.Z. Wang, Z.Z. Xia, Desiccant cooling air conditioning: a review, Renew. Sustain. Energy Rev. 10 (2006) 55–77.
- [10] R.Z. William Goetzler, J. Young, C. Johnson, U.S. D.O.E, in: Energy Savings Potential and RD&D Opportunities for Non-vapor-compression HVAC Technologies, 2014.
- [11] R. Xing, Y.X. Rao, W. TeGrotenhuis, N. Canfield, F. Zheng, D.W. Winiarski, W. Liu, Advanced thin zeolite/metal flat sheet membrane for energy efficient air dehumidification and conditioning, Chem. Eng. Sci. 104 (2013) 596–609.
- [12] O. Labban, T.Y. Chen, A.F. Ghoniem, V.J.H. Lienhard, L.K. Norford, Next-generation HVAC: prospects for and limitations of desiccant and membrane-based dehumidification and cooling, Appl. Energy 200 (2017) 330–346.
- [13] H.T. El-Dessouky, H.M. Ettouney, W. Bouhamra, A novel air conditioning systemmembrane air drying and evaporative cooling, Chem. Eng. Res. Des. 78 (2000) 999–1009.
- [14] B. Yang, W.X. Yuan, F. Gao, B.H. Guo, A review of membrane-based air dehumidification, Indoor Built Environ. 24 (2015) 11–26.
- [15] S.J. Metz, W.J.C. van de Ven, J. Potreck, M.H.V. Mulder, M. Wessling, Transport of water vapor and inert gas mixtures through highly selective and highly permeable polymer membranes, J. Membr. Sci. 251 (2005) 29–41.
- [16] D.T. Bui, A. Nida, K.C. Ng, K.J. Chua, Water vapor permeation and dehumidification performance of poly (vinyl alcohol)/lithium chloride composite membranes, J. Membr. Sci. 498 (2016) 254–262.
- [17] Q.L. Cheng, F.S. Pan, B. Chen, Z.Y. Jiang, Preparation and dehumidification performance of composite membrane with PVA/gelatin-silica hybrid skin layer, J. Membr. Sci. 363 (2010) 316–325.
- [18] A. Kudasheva, T. Kamiya, Y. Hirota, A. Ito, Dehumidification of air using liquid membranes with ionic liquids, J. Membr. Sci. 499 (2016) 379–385.
- [19] P. Scovazzo, Testing and evaluation of room temperature ionic liquid (RTIL) membranes for gas dehumidification, J. Membr. Sci. 355 (2010) 7–17.
- [20] H. Sijbesma, K. Nymeijer, R. van Marwijk, R. Heijboer, J. Potreck, M. Wessling, Flue gas dehydration using polymer membranes, J. Membr. Sci. 313 (2008) 263–276.
- [21] S.Z. Liu, F. Wang, T.L. Chen, Synthesis of poly(ether ether ketone)s with high content of sodium sulfonate groups as gas dehumidification membrane materials, Macromol. Rapid Commun. 22 (2001) 579–582.
- [22] K.E. O'Harra, I. Kammakakam, E.M. Devriese, D.M. Noll, J.E. Bara, E.M. Jackson, Synthesis and performance of 6FDA-based polyimide-ionenes and composites with ionic liquids as gas separation membranes, Membranes 9 (2019) 79–95.
- [23] W.L. Qiu, L.R. Xu, C.C. Chen, D.R. Paul, W.J. Koros, Gas separation performance of 6FDA-based polyimides with different chemical structures, Polymer 54 (2013) 6226–6235
- [24] S.A. Stern, Y. Mi, H. Yamamoto, A.K. Stclair, Structure permeability relationships of polyimide membranes - applications to the separation of gas-mixtures, J. Polym. Sci., Polym. Phys. Ed. 27 (1989) 1887–1909.
- [25] T. Matsuura, Y. Hasuda, S. Nishi, N. Yamada, Polyimide derived from 2,2'-bis (trifluoromethyl)-4,4'-diaminobiphenyl .1. Synthesis and characterization of polyimides prepared with 2,2-bis(3,4-Dicarboxyphenyl)Hexafluoropropane dianhydride or pyromellitic dianhydride, Macromolecules 24 (1991) 5001–5005.
- [26] J.W. Park, M. Lee, M.H. Lee, J.W. Liu, S.D. Kim, J.Y. Chang, S.B. Rhee, Synthesis and characterization of soluble alternating aromatic copolyimides, Macromolecules 27 (1994) 3459–3463.
- [27] S. Ioan, A.I. Cosutchi, C. Hulubei, D. Macocinschi, G. Ioanid, Surface and interfacial properties of poly(amic acid)s and polyimides, Polym. Eng. Sci. 47 (2007) 381–389.
- [28] H.T. Kwon, H.K. Jeong, A.S. Lee, H.S. An, J.S. Lee, Heteroepitaxially grown zeolitic imidazolate framework membranes with unprecedented propylene/propane separation performances, J. Am. Chem. Soc. 137 (2015) 12304–12311.

- [29] L.E. Stephans, A. Myles, R.R. Thomas, Kinetics of alkaline hydrolysis of a polyimide surface, Langmuir 16 (2000) 4706–4710.
- [30] H.C. Yu, J.W. Jung, J.Y. Choi, C.M. Chung, Kinetic study of low-temperature imidization of poly(amic acid)s and preparation of colorless, transparent polyimide films, J. Polym. Sci., Polym. Chem. Ed. 54 (2016) 1593–1602.
- [31] Y. Xu, A.L. Zhao, X.L. Wang, H. Xue, F.L. Liu, Influence of curing accelerators on the imidization of polyamic acids and properties of polyimide films, J. Wuhan Univ. Technol. 31 (2016) 1137–1143.
- [32] E.L. Johnson, The effects of reaction temperature and hydrolysis on polyamic acids and polyimides 15 (1971) 2825–2839.
- [33] S. Murray, C. Hillman, M. Pecht, Environmental aging and deadhesion of siloxanepolyimide-epoxy adhesive, Ieee T Compon Pack T 26 (2003) 524–531.
- [34] F.J. Campbell, Temperature-dependence of hydrolysis of polyimide wire insulation, Ieee T Electr Insul 20 (1985) 111–116.
- [35] R. Yeasmin, H. Zhang, J.X. Zhu, H. Kazemian, Pre-treatment and conditioning of chabazites followed by functionalization for making suitable additives used in antimicrobial ultra-fine powder coated surfaces, RSC Adv. 6 (2016) 88340–88349.

- [36] Y. Ding, B. Bikson, J.K. Nelson, Polyimide membranes derived from poly(amic acid) salt precursor polymers. 1. synthesis and characterization, Macromolecules 35 (2002) 905–911.
- [37] J. Komiyama, M. Satoh, W.Z. Zhang, A. Nodera, T. Kusano, K. Ogata, S. Takahashi, State of water in swollen membrane in relation to permeability, Polym. J. 23 (1991) 379–388.
- [38] S. Zeng, Q.W. Su, L.Z. Zhang, Molecular-level evaluation and manipulation of thermal conductivity, moisture diffusivity and hydrophobicity of a GO-PVP/PVDF composite membrane, Int. J. Heat Mass Tran. 152 (2020) 119508–119528.
- [39] L.Z. Zhang, Y.Y. Wang, C.L. Wang, H. Xiang, Synthesis and characterization of a PVA/LiCl blend membrane for air dehumidification, J. Membr. Sci. 308 (2008) 198–206
- [40] L.L. Cui, W.L. Qiu, D.R. Paul, W.J. Koros, Physical aging of 6FDA-based polyimide membranes monitored by gas permeability, Polymer 52 (2011) 3374–3380.